

SkyDiffusion: Street-to-Satellite Image Synthesis with Diffusion Models and BEV Paradigm

Junyan Ye^{1,2}, Jun He¹, Weijia Li^{1*}, Zhutao Lv¹, Jinhua Yu¹,
Haote Yang², Conghui He^{2,3*}

¹Sun Yat-Sen University, ²Shanghai AI Laboratory, ³Sensemte Research

{yejy53, hejun36, lvzht5, yujh56}@mail2.sysu.edu.cn,
liweij29@mail.sysu.edu.cn, {yanghaote, heconghui}@pjlab.org.cn

Abstract

Street-to-satellite image synthesis focuses on generating realistic satellite images from corresponding ground street-view images while maintaining a consistent content layout, similar to looking down from the sky. The significant differences in perspectives create a substantial domain gap between the views, making this cross-view generation task particularly challenging. In this paper, we introduce SkyDiffusion, a novel cross-view generation method for synthesizing satellite images from street-view images, leveraging diffusion models and Bird's Eye View (BEV) paradigm. First, we design a Curved-BEV method to transform street-view images to the satellite view, reformulating the challenging cross-domain image synthesis task into a conditional generation problem. Curved-BEV also includes a "Multi-to-One" mapping strategy for leveraging multiple street-view images within the same satellite coverage area, effectively solving the occlusion issues in dense urban scenes. Next, we design a BEV-controlled diffusion model to generate satellite images consistent with the street-view content, which also incorporates a light manipulation module to make the lighting conditions of the synthesized satellite images more flexible. Experimental results demonstrate that SkyDiffusion outperforms state-of-the-art methods on both suburban (CVUSA & CVACT) and urban (VIGOR-Chicago) cross-view datasets, with an average SSIM increase of 13.96% and a FID reduction of 20.54%, achieving realistic and content-consistent satellite image generation. The code and models of this work will be released at <https://opendatalab.github.io/skydiffusion/>

Introduction

Cross-view synthesis involves transformations between disparate viewpoints, such as from street-view images to satellite images and vice versa. This process is crucial for applications in urban planning (Li et al. 2023b), 3D reconstruction (Wang et al. 2021), virtual reality (Emmaneel et al. 2023), etc. The significant changes in street view and satellite perspectives result in drastically different appearances of objects, leading to a substantial disparity between different image domains. As shown in Fig 1 (a), in cross-view scenarios, building facades observed only in street view and rooftops observed only from satellite view are considered uncorrelated and drastically different features (Regmi and Borji 2018; Zhu et al. 2023). However, objects such as roads and lawns, which are below the viewpoint, can be observed in different views even

if they undergo some deformation, making them cross-view shared correlated information. The key to the challenging task of cross-view synthesis lies in bridging domain gaps, capturing cross-view relevant information, and generating realistic views with consistent content layouts.

In the field of cross-view synthesis, converting satellite images to street-view images has received extensive attention (Shi et al. 2022; Lu et al. 2020; Qian et al. 2023). Researchers have leveraged polar transformations (Toker et al. 2021) or geo-transformation (Lu et al. 2020) to bridge the gap from the satellite to the street view domain, and then employ Generative Adversarial Networks (GANs) to generate realistic street views. This paper focuses on the less explored yet equally challenging task of synthesizing satellite images from street-view images. Some researchers have used semantic segmentation priors to aid in synthesizing satellite images, achieving notable results (Tang et al. 2019). However, the semantic maps are often unavailable in real scenarios. Existing street-to-satellite image generation also lacks transformations such as polar or geo-transformation to fit the gap from the street view to the satellite domain. Moreover, as shown in Fig 1(b), existing methods on street-to-satellite image synthesis, which mostly rely on GANs, often result in lower-quality satellite images with unrealistic textures.

Recently, diffusion models have gained attention for their exceptional image synthesis (Ho, Jain, and Abbeel 2020; Zhang, Rao, and Agrawala 2023). Many studies have explored text-guided fine-tuning of diffusion models to top-down perspective from other views (Kothandaraman et al. 2023a; Ruiz et al. 2023). Additionally, novel view synthesis methods have been developed by training with multi-view images and camera poses (Liu et al. 2023; Shi et al. 2023a). Although current novel view synthesis techniques demonstrate satisfactory performance at the object level, their performance in cross-view generation for complex scenes with significant viewpoint differences remains suboptimal. A possible solution is to treat the this task as an image translation task (Li et al. 2023a; Parmar et al. 2024). However, as shown in Fig 1(b), due to the domain gap of different views, the resulting images are often realistic but not actual, with significant discrepancies between the synthesized satellite images and the actual corresponding street view content. In response to these challenges, this paper introduces SkyDiffusion, a street-to-satellite image synthesis method based on

*W. Li and C. He are the corresponding authors.

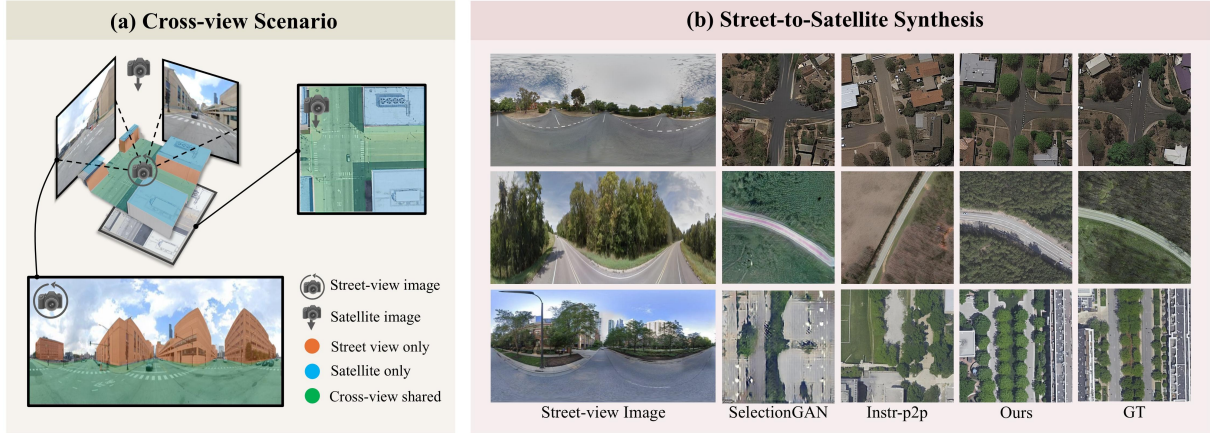


Figure 1: Illustration of the cross-view image synthesis task. (a) In the cross-view scenario, there are features unique to the street-view image, features exclusive to the satellite image, and shared correlated information observable from both views. (b) Comparison of our street-to-satellite image synthesis method with existing cross-view synthesis methods (e.g., SelectionGAN (Tang et al. 2019)) or image translation methods based on diffusion models (e.g., Instr-p2p (Brooks, Holynski, and Efros 2023)).

diffusion models and the BEV paradigm, similar to viewing from the sky. Unlike previous cross-view synthesis methods, our approach is based on a diffusion framework, enabling the generation of more realistic satellite images. We design a Curved-BEV method that transforms street-view images into satellite views, achieving domain alignment between different perspectives and facilitating content-consistent satellite image synthesis. To address the limited perception range of BEV in densely occluded urban scenarios, the Curved-BEV method also includes a Multi-to-One mapping strategy. Additionally, our BEV-controlled diffusion model incorporates a light manipulation module, making the lighting conditions of the synthesized satellite images more adaptable. Our main contributions are summarized as follows:

- We introduce SkyDiffusion, a novel street-to-satellite image synthesis method leveraging diffusion models and BEV paradigm to generate realistic and content-consistent satellite images.
- We design a Curved-BEV method to transform street-view images into satellite views for domain alignment. It also includes "Multi-to-One" mapping strategy to enhance BEV perception range in densely occluded urban areas.
- SkyDiffusion outperforms state-of-the-art methods on sub-urban (CVUSA, CVACT) and urban (VIGOR-Chicago) cross-view datasets, with a 13.96% SSIM increase and 20.54% FID reduction.

Related Work

Cross-view image synthesis involves generating realistic scenes images with significant viewpoint changes, primarily divided into satellite-to-street (Shi et al. 2022; Lu et al. 2020; Qian et al. 2023) and street-to-satellite generation (Regmi and Borji 2018, 2019). In this field, synthesizing satellite images from street views is a challenging yet important task. Regmi and Borji (2018) attempted to synthesize aerial views from a single street image, but the significant domain differences led to inconsistencies. Tang et al. (2019) used street-view images

and aerial semantic maps for image-to-image translation to synthesize target satellite images, but semantic maps are often unavailable in real scenarios. Additionally, the performance of GANs has also limited the quality of street-to-satellite image synthesis in previous studies.

BEV transformation is a perspective domain conversion technique similar to polar transformation (Shi et al. 2019; Toker et al. 2021) and geo-transformation (Lu et al. 2020), widely used in retrieval (Ye et al. 2024b), navigation (Li et al. 2022) and localization tasks (Song et al. 2023; Wang et al. 2023; Shi et al. 2023b). Traditional BEV transformation techniques, which rely on camera parameters (Sarlin et al. 2023) or depth estimation methods (Teng et al. 2024; Ye et al. 2024a), face challenges such as the difficulty in obtaining camera parameters and the high computational cost of depth estimation. Recently, some methods have been proposed to map street-view images to the BEV perspective using geometric relations at the image (Wang et al. 2023) or feature level (Shi et al. 2023b). However, such methods are based on the ground plane assumption, where all mapped points are located below the camera, limiting the mapping of upper street scene features and causing information loss. Furthermore, to our knowledge, no studies have yet explored the use of BEV methods for street-to-satellite image synthesis task.

Novel view synthesis based on diffusion models. Diffusion models have shown significant potential in recent studies on novel view synthesis (Kawar et al. 2023; Gao et al. 2024; Tseng et al. 2023). DreamBooth (Ruiz et al. 2023) and AerialDiffusion (Kothandaraman et al. 2023a) utilize text guidance to achieve top-down image generation by fine-tuning diffusion models. However, it is challenging to fully encapsulate the complexity of real-world scenes using textual information alone. Zero-1-to-3 (Liu et al. 2023) and Zero 123++ (Shi et al. 2023a) use multi-view images and camera poses to guide diffusion models in learning object structures and textures, enabling new viewpoint synthesis. However, these methods are limited to object-level tasks with strong viewpoint correlations and struggle to handle the sig-

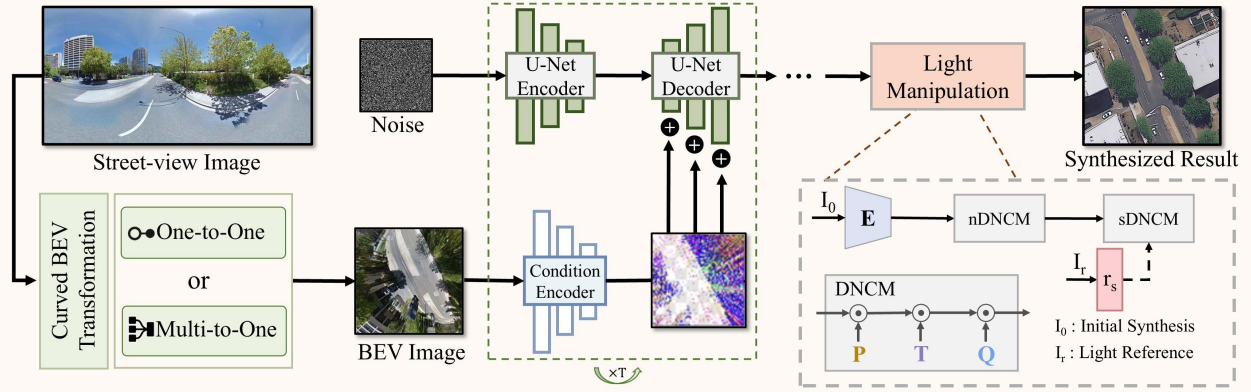


Figure 2: Overview of the proposed SkyDiffusion framework, including the curved BEV transformation and BEV-controlled diffusion model with light manipulation.

nificant viewpoint changes in cross-view generation. Besides, diffusion-based image-to-image translation methods can also generate realistic satellite images (Li et al. 2023a; Brooks, Holynski, and Efros 2023; Zhang, Rao, and Agrawala 2023). However, the substantial domain gap between street-view images and satellite images presents a significant challenge in generating content-consistent satellite images.

Methods

As illustrated in Fig. 2, this paper introduces SkyDiffusion, a novel method for synthesizing satellite images from corresponding street-view images. It initially applies a curved BEV transformation to the input street-view images, converting the perspective to a top-down view using either one-to-one or multi-to-one mappings. Subsequently, the BEV-Controlled diffusion model with light manipulation is employed for the controlled synthesis of satellite images. Following this, we detail our network training process.

Curved BEV Transformation

One-to-One BEV. Existing BEV methods based on ground plane assumptions ($P(x, y, z = 0)$) and geometric relationships achieve the mapping from street view to the BEV plane (Shi et al. 2023b; Wang et al. 2023). However, this assumption fails to map the content above the street-view image and results in noticeable distortion as points move away from the center area. Thus, we propose an enhanced curved BEV transformation to better capture cross-view information and address this issue.

As shown in Fig. 3 (a), we use $P(i, j)$ to denote an index on the BEV space, and $P(x, y, z)$ to illustrate a point in a three-dimensional coordinate system with the camera on the z-axis. We assume that the BEV plane is an upward curved surface, with the height (z-axis) increasing rapidly as the 3D points move away from the center (the central part of Fig 3(a)). The following equation formulates the relationship between $P(x, y, z)$ and $P(i, j)$, where d_{norm} represents the normalized distance from the center, d_{max} is the maximum distance from the center, and λ is a scaling factor.

$$\begin{cases} x = j - \frac{l}{2}, & y = \frac{l}{2} - i \\ z = d_{norm}^4 \times \lambda = \left(\frac{\sqrt{x^2 + y^2}}{d_{max}} \right)^4 \times \lambda \end{cases} \quad (1)$$

Furthermore, we can convert $P(x, y, z)$ to spherical coordinates $P(\theta, \varphi)$. Based on the equirectangular projection properties of street view images, $P(\theta, \varphi)$ corresponds to the panorama image index $P(u, v)$. This allows us to establish the mapping relationship between $P(x, y, z)$ and $P(u, v)$ from the following equation, where H represents the camera height, and w, h represent the width and height of the street image. More details are in the supplementary material.

$$\begin{cases} u = [\arctan2(y, x) + \pi] \frac{w}{2\pi} \\ v = \left[\frac{\pi}{2} + \arctan2(z - H, \sqrt{x^2 + y^2}) \right] \frac{h}{\pi} \end{cases} \quad (2)$$

Following Eq. 1 and Eq. 2, we achieve the projection from the street-view image to the bird's eye view without requiring camera calibration parameters or depth estimation methods (Teng et al. 2024; Ye et al. 2024a) (Fig. 3 (b)). This effectively maps upper street view features like distant roads and buildings. Since the mapping relationship for each transformation is fixed, the computational overhead is minimal.

Multi-to-One BEV. Due to the limitations imposed by dense buildings on street view observations, the BEV sensing range is very limited in urban datasets like VIGOR. To address this, we propose a "Multi-to-one" BEV mapping method that unifies multiple street view BEV mappings results BEV_{cam_k} into a single satellite coordinate system based on the relationships of camera position (Fig. 3 (c)). We use a simple semantic segmentation network to identify and discard the regions with severe BEV distortion, typically those obstructed by buildings. We select the street view mapping result closest to the capture point for overlapping areas following Eq. 3, where $BEV(x, y)$ represents the unified BEV space corresponding to the satellite image, x, y corresponds to the index position of the BEV plane, Δx_k and Δy_k represent the offset of the street-view image from the satellite

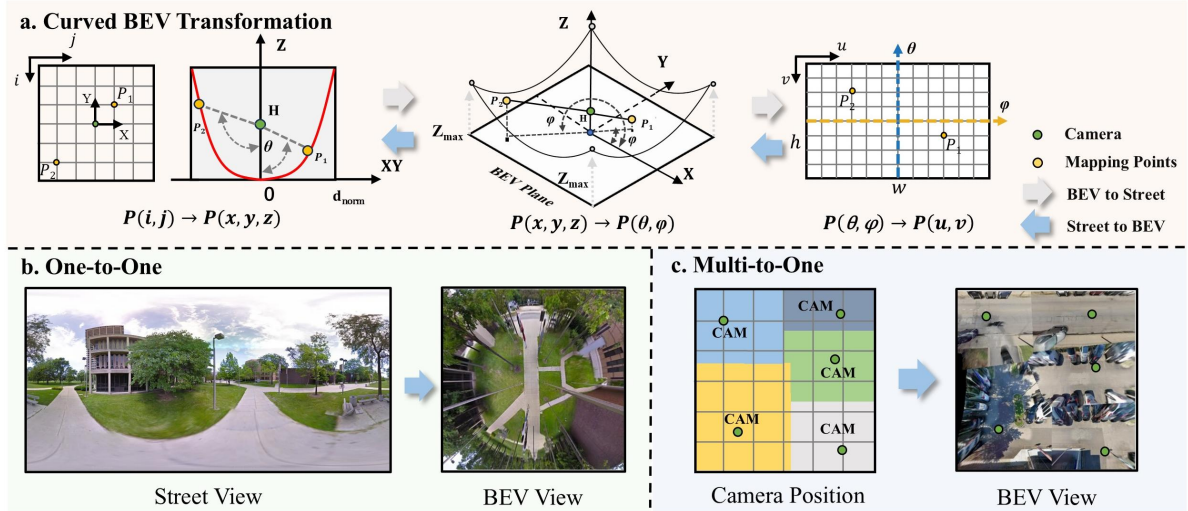


Figure 3: Schematic of the curved BEV transformation. The upper part (a) details the transformation process, highlighting the two mapping points at the top and bottom of the street view. The lower parts (b) and (c) present the results of One-to-One and Multi-to-One BEV transformations, respectively.

center, and x_{cam_i} and y_{cam_i} represent the coordinates of camera position in the satellite coordinate system.

$$\begin{cases} \text{BEV}(x, y) = \text{BEV}_{\text{cam}_k}(x - \Delta x_k, y - \Delta y_k) \\ k = \arg \min_i \sqrt{(x - x_{\text{cam}_i})^2 + (y - y_{\text{cam}_i})^2} \end{cases} \quad (3)$$

This enables us to synthesize large-scale scenes using street-view images with limited local information.

BEV-Controlled Synthesis with Light Manipulation

Curved BEV controlled synthesis. Image diffusion models progressively denoise images and generate samples from the training domain. The denoising process can occur in pixel space or in a latent space encoded from training data. Inspired by ControlNet (Zhang, Rao, and Agrawala 2023), we enhance the control over the generated aerial views by replicating the SD module, enabling the transformed BEV images to effectively guide the synthesis process. Specifically, we first use a small encoder to capture the cross-view associative information of the input BEV image I_{bev} such as road directions and building positions, to achieve BEV image feature embedding c_{bev} . Notably, considering the potential feature distortions in BEV images, we employ a spatial attention mechanism to enhance feature capture while suppressing distorted features.

$$c_{\text{bev}} = \mathcal{E}(I_{\text{bev}}). \quad (4)$$

Subsequently, by using zero convolution layers and replicating the encoder and middle block structures and weights from the SD module, the extracted BEV features are injected into another SD module. Guided by the BEV image, the diffusion model incorporates cross-view associative information, synthesizing aerial views with consistent content.

Light Manipulation. Given the differences in perspectives and timing between satellite and street images, there is no direct correlation in lighting conditions. To address

this, we designed a light manipulation module to make the lighting conditions of the synthesized satellite images more adaptable. We employ the DNCM for modeling deterministic color mapping (Ke et al. 2023). Initially, we use nDNCM to obtain the "image content information" I_c from the preliminary synthesis results I_0 of the satellite images. Then, we input the lighting and color style r_s obtained from the reference aerial view into sDNCM for lighting transfer.

$$\begin{cases} I_s = \text{sDNCM}(n\text{DNCM}(I_0, I_c), r_s) \\ \text{DNCM}(I, T) = (I_{h \times w, 3} \cdot P_{3, k}) \cdot T_{k, k} \cdot Q_{k, 3} \end{cases} \quad (5)$$

I_c and r_s are the content information and color reference information extracted by the encoder E , as shown in Fig. 2. The DNCM module internally includes $P_{3, k}$ and $Q_{k, 3}$, which represent the color embedding and recovery matrices, respectively. Here, k represents the embedding dimension. The adaptive color mapping matrix $T_{k, k}$ is also obtained through the encoder. Notably, the lighting adjustment module is independent of the satellite image synthesis, meaning that satellite images can be generated without relying on this module. We obtain lighting information from randomly selected satellite images in the training set, and standard images can also be used as lighting control conditions.

Network Training

Loss Function. We train the BEV-controlled synthesis of satellite images and the light manipulation module in two separate stages. Given a set of cross-view image data, the image diffusion algorithm gradually adds noise to the satellite image, generating a noisy satellite image Z_t . It then learns a network ϵ_θ to predict the noise added to the noisy satellite image Z_t based on the given BEV image as the conditional input. Since text cannot fully describe the street view scene, our cross-view image synthesis is essentially an image-conditioned synthesis task, with text not being our

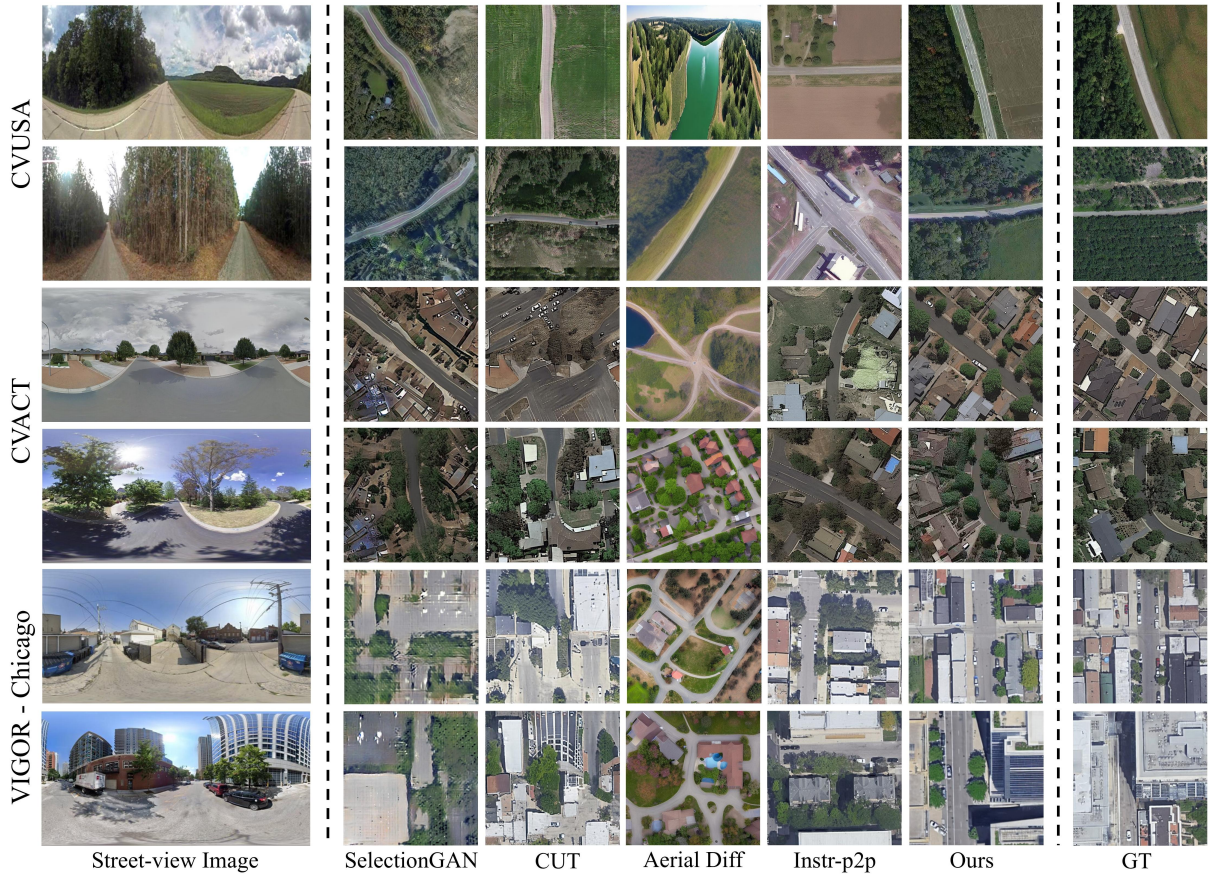


Figure 4: Qualitative Comparison of Synthesis Results. The first and second rows present the results on the CVUSA dataset, while the third and fourth rows display the results on the CVACT dataset. The fifth and sixth rows showcase the visualized outcomes on the VIGOR-Chicago dataset.

optimization target. This helps the model focus on generating satellite images based on the BEV conditions.

$$\mathcal{L} = \mathbb{E}_{sat_0, t, c_{bev}, \epsilon \sim \mathcal{N}(0, 1)} \left[\|\epsilon - \epsilon_\theta(sat_t, t, c_{bev})\|_2^2 \right] \quad (6)$$

The loss \mathcal{L} is the learning objective of the diffusion model, where t represents the time step.

Following previous work (Ke et al. 2022, 2023), we apply different LUT filters to the satellite images to simulate the results under various lighting conditions for training the light manipulation module. During training, we use L2 consistency loss \mathcal{L}_{con} to maintain image content consistency and L1 reconstruction loss \mathcal{L}_{rec} to learn color style transfer.

Implementation Details. We implement SkyDiffusion using the pre-trained Stable Diffusion v1.5 model (Rombach et al. 2022), with an unlocked diffusion decoder and a classifier-free guidance scale of 9.0 (Ho and Salimans 2022). Final inference sampling uses 50 steps with the DDIM strategy (Song, Meng, and Ermon 2021). Training is on eight NVIDIA A100 GPUs with a batch size of 128 for 100 epochs. For light manipulation, the reference satellite image is randomly selected from normally toned images in the training

set, and the DNCM mapping matrix parameter k is set to 32 (details in Supplementary Material).

Experiments

In this section, we introduce the three datasets utilized and the experimental setup. We then conduct both qualitative and quantitative comparisons of SkyDiffusion with state-of-the-art cross-view synthesis methods. Finally, we perform ablation studies to evaluate the effectiveness of each module.

Datasets

CVUSA & CVACT (Suburban dataset). CVUSA (Workman, Souvenir, and Jacobs 2015) and CVACT (Liu and Li 2019) are two widely used cross-view datasets. They contain centrally aligned satellite and street-view images from regions in the United States and Canberra, Australia, respectively, with a one-to-one mapping relationship. The data primarily consists of suburban scenes characterized by relatively low-rise buildings and open views. The CVUSA dataset's training and testing sets are randomly split, while the CVACT dataset is split by region.

VIGOR-Chicago (Urban dataset). VIGOR-Chicago (Zhu, Yang, and Chen 2021) is a subset of the VIGOR dataset,

Method	CVUSA				CVACT				VIGOR-Chicago			
	FID (↓)	SSIM (↑)	PSNR (↑)	LPIPS (↓)	FID (↓)	SSIM (↑)	PSNR (↑)	LPIPS (↓)	FID (↓)	SSIM (↑)	PSNR (↑)	LPIPS (↓)
X-Seq	161.16	0.084	11.97	0.706	190.12	0.042	12.41	0.661	-	-	-	-
CDTE	122.84	0.143	10.01	0.694	160.81	0.091	12.59	0.663	-	-	-	-
SelectionGAN	116.57	0.129	12.38	0.742	100.21	0.116	12.04	0.684	149.53	0.127	11.77	0.778
Aerial Diff	136.18	0.103	10.06	0.855	127.29	0.108	10.24	0.878	123.16	0.141	11.49	0.831
HawkI	90.98	0.114	11.09	0.783	135.75	0.112	10.97	0.764	123.47	0.124	9.67	0.752
CUT	72.83	0.121	12.09	0.687	62.22	0.102	13.11	0.664	69.42	0.169	13.66	0.665
img2img-turbo	77.95	0.127	12.64	0.685	73.24	0.103	12.19	0.679	80.10	0.135	11.28	0.690
Instr-p2p	38.01	0.138	12.29	0.697	49.62	0.116	12.51	0.682	50.30	0.163	10.62	0.689
Ours	29.18	0.168	14.58	0.635	35.51	0.123	13.58	0.657	45.29	0.186	11.69	0.661

Table 1: Quantitative comparison of different methods on CVUSA, CVACT and VIGOR-Chicago.

containing cross-view image pairs collected from Chicago urban area. In this dataset, the street panorama and satellite images are not centrally aligned, and multiple street-view images cover the same satellite image area, with overlapping regions between different satellite images, forming a multi-to-one mapping relationship. All input street images are set to 512×1024 pixels, with the center column aligned to the north. Unlike previous methods that synthesize low-resolution satellite images (64×64 or 256×256 pixels), this experiment aims to meet practical needs by generating higher-resolution satellite images (512×512 pixels). In the Curved-BEV transformation, λ is set to 3 and H to 1.5 for CVUSA and CVACT datasets. For the VIGOR-Chicago dataset, λ is set to 10, with H unchanged. The Curved-BEV transformation results in street images that match the size of the satellite images.

Experimental Setup

We compared our method on three datasets with several state-of-the-art cross-view synthesis methods, including the commonly used cross-view satellite synthesis methods X-Seq (Regmi and Borji 2018), SelectionGAN (without semantic masks) (Tang et al. 2019), and CDTE (Toker et al. 2021), image translation methods such as the GAN-based CUT (Park et al. 2020) and diffusion-based Instruct pix2pix (Instr-p2p) (Brooks, Holynski, and Efros 2023) and img2img-turbo (Parmar et al. 2024), as well as novel view synthesis methods like Aerial Diff (Kothandaraman et al. 2023a) and HawkI (Kothandaraman et al. 2023b).

Except for the fine-tuned diffusion model, which requires brief textual descriptions, all other models use the same street-view input for a fair comparison.

Following previous work (Lu et al. 2020; Toker et al. 2021; Regmi and Borji 2018), we employ commonly used metrics such as SSIM, PSNR and LPIPS to evaluate the content consistency of the synthesized images, and use FID (Heusel et al. 2017) to assess the realism of images.

Comparison with State-of-the-Art Methods

On the suburban CVUSA and CVACT datasets, our SkyDiffusion method achieved the outstanding results, as shown in Table 1. Compared to state-of-the-art methods, it reduced FID by 25.83% and increased SSIM by 13.89%, demonstrating its superiority in synthesizing realistic and consistent satellite

images. The visual results in Fig. 4 show that GAN-based cross-view methods generate excessive artifacts and blurriness. While diffusion-based methods such as Aerial Diff and Instr-p2p produce highly realistic aerial views, they lack content correlation with the street-view images. In contrast, our method benefits from BEV perspective transformation, enabling effective capture of cross-view associative information. SkyDiffusion generates realistic images with consistent content layout, including road direction, tree placement, and building distribution. Additional visual results can be found in the supplementary materials.

In the urban VIGOR-Chicago dataset, SkyDiffusion reduced FID by 9.96% and improved SSIM by 14.11% compared to the state-of-the-art method, as shown in Table 1. For fair comparison, the VIGOR results for SkyDiffusion use only a single street-view image. The results using Multi-to-One BEV generation with multiple street-view images can be found in the ablation study. The visual results in Fig. 4 show that our method maintains consistent associative information such as crosswalks and lanes. While the non-associative information on building rooftops cannot be consistently generated, it still produces reasonable and realistic results.

Ablation Study

Curved-BEV controlled synthesis. We conducted ablation experiments on the three datasets, with results shown in Table 2. Compared to directly using street-view images as input, the Curved-BEV method improves performance across multiple metrics by transforming street-view images into satellite views for domain alignment. This indicates that the Curved-BEV method aids in synthesizing more content-consistent satellite images. Furthermore, the Multi-to-one method further improves metrics compared to the one-to-one mapping, demonstrating its effectiveness in dense urban scenes. As shown in the visual results in Figure 5, using multiple street-view images for multi-to-one BEV mapping effectively addresses occlusions from tall objects like trees and buildings. This method effectively enhances the BEV sensing range in urban environments, facilitating the generation of large-scale satellite scenes. Additional ablation study results can be found in the supplementary materials.

Light manipulation. The ablation experiments in Table 3 indicate that the Light Manipulation module aligns the light-

Method	FID (↓)	SSIM (↑)	PSNR (↑)	LPIPS (↓)
CVUSA				
Baseline	32.45	0.149	12.63	0.650
Ours (C-BEV)	29.18	0.168	14.58	0.635
CVACT				
Baseline	62.21	0.115	11.95	0.682
Ours (C-BEV)	35.51	0.123	13.58	0.657
VIGOR-Chicago				
Baseline	53.27	0.170	10.38	0.666
Ours (C-BEV)	45.29	0.186	11.69	0.661
Ours (C-BEV Multi)	31.90	0.205	11.15	0.651

Table 2: Ablation study of the Curved-BEV module. "Baseline" represents directly using street-view image, "C-BEV" denotes using Curved-BEV transformation, and "Multi" stands for Multi-to-One strategy.

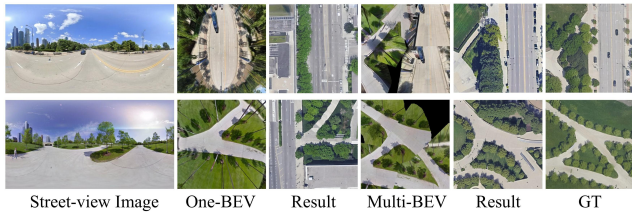


Figure 5: Qualitative comparison of synthesis results for One-to-one and Multi-to-one BEV.

ing conditions of the synthesized images with those of the target domain images, improving SSIM and PSNR metrics. This is because satellites typically capture large areas with relatively uniform overall brightness. Using a small satellite image slice as a reference effectively captures the lighting conditions at the time of capture. Due to the dispersed distribution of the CVUSA data and the more complex lighting conditions, the improvements are not as pronounced as on other datasets. The light processing module maintains the original image content while providing more flexible lighting conditions for the synthesized satellite images. More visualization results can be found in the supplementary material.

Method	FID (↓)	SSIM (↑)	PSNR (↑)	LPIPS (↓)
CVUSA				
Ours (w/o light)	29.02	0.167	14.07	0.643
Ours	29.18	0.168	14.58	0.635
CVACT				
Ours (w/o light)	36.48	0.117	12.85	0.665
Ours	35.51	0.123	13.58	0.657
VIGOR-Chicago				
Ours (w/o light)	46.77	0.179	10.46	0.666
Ours	45.29	0.186	11.69	0.661

Table 3: Ablation study of the light manipulation module.

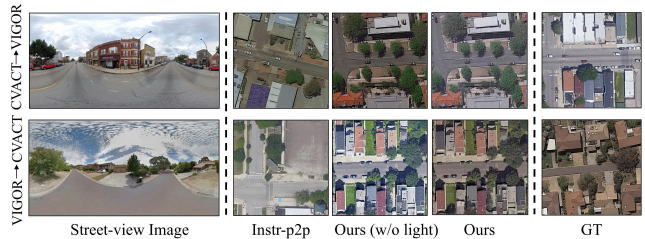


Figure 6: Synthesis results for cross-dataset generalization.

Method	FID (↓)	SSIM (↑)	PSNR (↑)	LPIPS (↓)
CVACT → VIGOR-Chicago				
Instr-p2p	100.80	0.152	9.14	0.717
Ours (w/o light)	89.76	0.155	9.45	0.739
Ours	63.04	0.162	11.24	0.723
VIGOR-Chicago → CVACT				
Instr-p2p	121.29	0.113	8.90	0.759
Ours (w/o light)	107.58	0.116	8.76	0.751
Ours	100.58	0.121	11.36	0.714

Table 4: Cross-dataset generalization assessment.

Cross-Dataset Generalization

We trained the model on CVACT and tested it on the VIGOR-Chicago, and vice versa, to evaluate cross-dataset generation capability, as shown in Table 4. Compared to Instruct pix2pix, our method (w/o light) demonstrates superior performance across metrics. Figure 6 shows the synthesis results for cross-dataset generalization. Our method effectively preserves scene content such as road directions and intersections. However, due to the distinct city styles of the CVACT and VIGOR datasets and the fact that the model was trained on a single dataset, there are noticeable differences in elements such as buildings and lighting conditions. The aim of this task is not to generate identical satellite images but to create scenes with consistent content layouts while exhibiting distinctly different styles. Additionally, we can flexibly use the light manipulation module to obtain light information from a random image in the target dataset's training set, better matching the target domain's lighting conditions.

Conclusion

In this study, we introduce SkyDiffusion, a novel approach specifically designed for street images to satellite images cross-view synthesis. SkyDiffusion operates solely with street images as input, utilizing a BEV Paradigm and diffusion models to generate satellite images. SkyDiffusion achieves state-of-the-art performance in both content consistency and image realism on suburban and urban cross-view datasets, demonstrating its superior capabilities in cross-view synthesis tasks. The satellite and street-view domains bridging method, Curved-BEV, within this approach also holds valuable insights for tasks such as cross-view retrieval and geolocation. In the future work, we plan to extend our method to more cities and further refine it for specific downstream applications, such as urban planning and virtual tourism.

References

Brooks, T.; Holynski, A.; and Efros, A. A. 2023. Instruct-pix2pix: Learning to follow image editing instructions. In *Proceedings of the IEEE/CVF Conference on Computer Vision and Pattern Recognition*, 18392–18402.

Emmeneel, R.; Oswald, M. R.; de Haan, S.; and Datcu, D. 2023. Cross-View Outdoor Localization in Augmented Reality by Fusing Map and Satellite Data. *Applied Sciences*, 13(20): 11215.

Gao, R.; Chen, K.; Xie, E.; Lanqing, H.; Li, Z.; Yeung, D.-Y.; and Xu, Q. 2024. MagicDrive: Street View Generation with Diverse 3D Geometry Control. In *International Conference on Learning Representations*.

Heusel, M.; Ramsauer, H.; Unterthiner, T.; Nessler, B.; and Hochreiter, S. 2017. GANs Trained by a Two Time-Scale Update Rule Converge to a Local Nash Equilibrium. In Guyon, I.; Luxburg, U. V.; Bengio, S.; Wallach, H.; Fergus, R.; Vishwanathan, S.; and Garnett, R., eds., *Advances in Neural Information Processing Systems*, volume 30. Curran Associates, Inc.

Ho, J.; Jain, A.; and Abbeel, P. 2020. Denoising Diffusion Probabilistic Models. In Larochelle, H.; Ranzato, M.; Hadsell, R.; Balcan, M.; and Lin, H., eds., *Advances in Neural Information Processing Systems*, volume 33, 6840–6851. Curran Associates, Inc.

Ho, J.; and Salimans, T. 2022. Classifier-free diffusion guidance. *arXiv preprint arXiv:2207.12598*.

Kawar, B.; Zada, S.; Lang, O.; Tov, O.; Chang, H.; Dekel, T.; Mosseri, I.; and Irani, M. 2023. Imagic: Text-based real image editing with diffusion models. In *Proceedings of the IEEE/CVF Conference on Computer Vision and Pattern Recognition*, 6007–6017.

Ke, Z.; Liu, Y.; Zhu, L.; Zhao, N.; and Lau, R. W. 2023. Neural preset for color style transfer. In *Proceedings of the IEEE/CVF Conference on Computer Vision and Pattern Recognition*, 14173–14182.

Ke, Z.; Sun, C.; Zhu, L.; Xu, K.; and Lau, R. W. 2022. Harmonizer: Learning to perform white-box image and video harmonization. In *European Conference on Computer Vision*, 690–706. Springer.

Kothandaraman, D.; Zhou, T.; Lin, M.; and Manocha, D. 2023a. Aerial Diffusion: Text Guided Ground-to-Aerial View Synthesis from a Single Image using Diffusion Models. In *SIGGRAPH Asia 2023 Technical Communications*, 1–4.

Kothandaraman, D.; Zhou, T.; Lin, M. C.; and Manocha, D. 2023b. HawkI: Homography&Mutual Information Guidance for 3D-free Single Image to Aerial View.

Li, B.; Xue, K.; Liu, B.; and Lai, Y.-K. 2023a. Bbdm: Image-to-image translation with brownian bridge diffusion models. In *Proceedings of the IEEE/CVF conference on computer vision and pattern Recognition*, 1952–1961.

Li, W.; Lai, Y.; Xu, L.; Xiangli, Y.; Yu, J.; He, C.; Xia, G.-S.; and Lin, D. 2023b. OmniCity: Omnipotent city understanding with multi-level and multi-view images. In *Proceedings of the IEEE/CVF Conference on Computer Vision and Pattern Recognition*, 17397–17407.

Li, Z.; Wang, W.; Li, H.; Xie, E.; Sima, C.; Lu, T.; Qiao, Y.; and Dai, J. 2022. Bevformer: Learning bird's-eye-view representation from multi-camera images via spatiotemporal transformers. In *European conference on computer vision*, 1–18. Springer.

Liu, L.; and Li, H. 2019. Lending orientation to neural networks for cross-view geo-localization. In *Proceedings of the IEEE/CVF conference on computer vision and pattern recognition*, 5624–5633.

Liu, R.; Wu, R.; Van Hoorick, B.; Tokmakov, P.; Zakharov, S.; and Vondrick, C. 2023. Zero-1-to-3: Zero-shot one image to 3d object. In *Proceedings of the IEEE/CVF International Conference on Computer Vision*, 9298–9309.

Lu, X.; Li, Z.; Cui, Z.; Oswald, M. R.; Pollefeys, M.; and Qin, R. 2020. Geometry-aware satellite-to-ground image synthesis for urban areas. In *Proceedings of the IEEE/CVF Conference on Computer Vision and Pattern Recognition*, 859–867.

Park, T.; Efros, A. A.; Zhang, R.; and Zhu, J.-Y. 2020. Contrastive learning for unpaired image-to-image translation. In *Computer Vision–ECCV 2020: 16th European Conference, Glasgow, UK, August 23–28, 2020, Proceedings, Part IX 16*, 319–345. Springer.

Parmar, G.; Park, T.; Narasimhan, S.; and Zhu, J.-Y. 2024. One-Step Image Translation with Text-to-Image Models. *arXiv preprint arXiv:2403.12036*.

Qian, M.; Xiong, J.; Xia, G.-S.; and Xue, N. 2023. Sat2Density: Faithful Density Learning from Satellite-Ground Image Pairs. In *Proceedings of the IEEE/CVF International Conference on Computer Vision (ICCV)*, 3683–3692.

Regmi, K.; and Borji, A. 2018. Cross-view image synthesis using conditional gans. In *Proceedings of the IEEE conference on Computer Vision and Pattern Recognition*, 3501–3510.

Regmi, K.; and Borji, A. 2019. Cross-view image synthesis using geometry-guided conditional gans. *Computer Vision and Image Understanding*, 187: 102788.

Rombach, R.; Blattmann, A.; Lorenz, D.; Esser, P.; and Ommer, B. 2022. High-resolution image synthesis with latent diffusion models. In *Proceedings of the IEEE/CVF conference on computer vision and pattern recognition*, 10684–10695.

Ruiz, N.; Li, Y.; Jampani, V.; Pritch, Y.; Rubinstein, M.; and Aberman, K. 2023. Dreambooth: Fine tuning text-to-image diffusion models for subject-driven generation. In *Proceedings of the IEEE/CVF Conference on Computer Vision and Pattern Recognition*, 22500–22510.

Sarlin, P.-E.; DeTone, D.; Yang, T.-Y.; Avetisyan, A.; Straub, J.; Malisiewicz, T.; Bulò, S. R.; Newcombe, R.; Kotschieder, P.; and Balntas, V. 2023. OrienterNet: Visual Localization in 2D Public Maps with Neural Matching. In *Proceedings of the IEEE/CVF Conference on Computer Vision and Pattern Recognition*, 21632–21642.

Shi, R.; Chen, H.; Zhang, Z.; Liu, M.; Xu, C.; Wei, X.; Chen, L.; Zeng, C.; and Su, H. 2023a. Zero123++: a single image to consistent multi-view diffusion base model. *arXiv preprint arXiv:2310.15110*.

Shi, Y.; Campbell, D.; Yu, X.; and Li, H. 2022. Geometry-guided street-view panorama synthesis from satellite imagery. *IEEE Transactions on Pattern Analysis and Machine Intelligence*, 44(12): 10009–10022.

Shi, Y.; Liu, L.; Yu, X.; and Li, H. 2019. Spatial-aware feature aggregation for image based cross-view geo-localization. *Advances in Neural Information Processing Systems*, 32.

Shi, Y.; Wu, F.; Perincherry, A.; Vora, A.; and Li, H. 2023b. Boosting 3-DoF Ground-to-Satellite Camera Localization Accuracy via Geometry-Guided Cross-View Transformer. In *Proceedings of the IEEE/CVF International Conference on Computer Vision*, 21516–21526.

Song, J.; Meng, C.; and Ermon, S. 2021. Denoising Diffusion Implicit Models. In *International Conference on Learning Representations*.

Song, Z.; Lu, J.; Shi, Y.; et al. 2023. Learning Dense Flow Field for Highly-accurate Cross-view Camera Localization. *Advances in Neural Information Processing Systems*, 36.

Tang, H.; Xu, D.; Sebe, N.; Wang, Y.; Corso, J. J.; and Yan, Y. 2019. Multi-channel attention selection gan with cascaded semantic guidance for cross-view image translation. In *Proceedings of the IEEE/CVF conference on computer vision and pattern recognition*, 2417–2426.

Teng, Z.; Zhang, J.; Yang, K.; Peng, K.; Shi, H.; Reiß, S.; Cao, K.; and Stiefelhagen, R. 2024. 360BEV: Panoramic Semantic Mapping for Indoor Bird’s-Eye View. In *Proceedings of the IEEE/CVF Winter Conference on Applications of Computer Vision*, 373–382.

Toker, A.; Zhou, Q.; Maximov, M.; and Leal-Taixé, L. 2021. Coming down to earth: Satellite-to-street view synthesis for geo-localization. In *Proceedings of the IEEE/CVF Conference on Computer Vision and Pattern Recognition*, 6488–6497.

Tseng, H.-Y.; Li, Q.; Kim, C.; Alsisan, S.; Huang, J.-B.; and Kopf, J. 2023. Consistent View Synthesis with Pose-Guided Diffusion Models. In *Proceedings of the IEEE/CVF Conference on Computer Vision and Pattern Recognition*, 16773–16783.

Wang, D.; Cui, X.; Chen, X.; Zou, Z.; Shi, T.; Salcudean, S.; Wang, Z. J.; and Ward, R. 2021. Multi-view 3d reconstruction with transformers. In *Proceedings of the IEEE/CVF international conference on computer vision*, 5722–5731.

Wang, X.; Xu, R.; Cui, Z.; Wan, Z.; and Zhang, Y. 2023. Fine-Grained Cross-View Geo-Localization Using a Correlation-Aware Homography Estimator. *Advances in Neural Information Processing Systems*, 36.

Workman, S.; Souvenir, R.; and Jacobs, N. 2015. Wide-area image geolocalization with aerial reference imagery. In *Proceedings of the IEEE International Conference on Computer Vision*, 3961–3969.

Ye, J.; Luo, Q.; Yu, J.; Zhong, H.; Zheng, Z.; He, C.; and Li, W. 2024a. SG-BEV: Satellite-Guided BEV Fusion for Cross-View Semantic Segmentation. *arXiv preprint arXiv:2404.02638*.

Ye, J.; Lv, Z.; Li, W.; Yu, J.; Yang, H.; Zhong, H.; and He, C. 2024b. Cross-view image geo-localization with Panorama-BEV Co-Retrieval Network. *arXiv preprint arXiv:2408.05475*.

Zhang, L.; Rao, A.; and Agrawala, M. 2023. Adding Conditional Control to Text-to-Image Diffusion Models. In *Proceedings of the IEEE/CVF International Conference on Computer Vision (ICCV)*, 3836–3847.

Zhu, S.; Yang, T.; and Chen, C. 2021. Vigor: Cross-view image geo-localization beyond one-to-one retrieval. In *Proceedings of the IEEE/CVF Conference on Computer Vision and Pattern Recognition*, 3640–3649.

Zhu, Y.; Chen, S.; Lu, X.; and Chen, J. 2023. Cross-View Image Synthesis From a Single Image With Progressive Parallel GAN. *IEEE Transactions on Geoscience and Remote Sensing*.